



	Optimizing fast-scan cyclic voltammetry for the analysis of 17- $\beta$ estradiol and its interactions with dopamine. Supplément		
Auteurs: Authors:	Edith Mariez, & Raphaël Trouillon		
Date:			
Туре:	Article de revue / Article		
Référence: Citation:	Mariez, E., & Trouillon, R. Optimizing fast-scan cyclic voltammetry for the analysis of $17-\beta$ estradiol and its interactions with dopamine. Neuroelectronics, 2(1), 0004 (26 pages). <a href="https://www.elspublishing.com/papers/j/1884284783601410048.html">https://www.elspublishing.com/papers/j/1884284783601410048.html</a>		

## Document en libre accès dans PolyPublie Open Access document in PolyPublie

<b>URL de PolyPublie:</b> PolyPublie URL:	https://publications.polymtl.ca/64716/
Version:	Matériel supplémentaire / Supplementary material Révisé par les pairs / Refereed
<b>Conditions d'utilisation:</b> Terms of Use:	Creative Commons Attribution 4.0 International (CC BY)

## Document publié chez l'éditeur officiel Document issued by the official publisher

<b>Titre de la revue:</b> Journal Title:	Neuroelectronics (vol. 2, no. 1)
<b>Maison d'édition:</b> Publisher:	ELSP
<b>URL officiel:</b> Official URL:	https://www.elspublishing.com/papers/j/1884284783601410048.html
Mention légale: Legal notice:	©2025 by the authors. Published by ELSP. This work is licensed under a Creative Commons Attribution 4.0 International License, which permits unrestricted use, distribution, and reproduction in any medium provided the original work is properly cited.

ELSP Neuroelectronics

https://doi.org/10.55092/neuroelectronics20250004

### **Supporting Information**

# Optimizing fast-scan cyclic voltammetry for the analysis of $17-\beta$ Estradiol and its interactions with dopamine

Edith Mariez<sup>1</sup> and Raphaël Trouillon<sup>1,2,3,\*</sup>

- <sup>1</sup> Electrical Engineering Department, Polytechnique Montréal, Montréal, Canada
- <sup>2</sup> TransMedTech Institute, Montréal, Canada
- <sup>3</sup> SNC Research Group, Montréal, Canada
- \* Correspondence author; E-mail: raphael.trouillon@polymtl.ca.

#### 1. Microscopic image of a carbon fiber

A micrograph of the tip of a CFME was taken with scanning electron microscopy (SEM). A Quanta FEG was used, with a 2.0 kV voltage. The micrograph (Figure 1) shows the surface structure of the carbon fiber, and the tip of the electrode, cut to length with a scalpel blade.

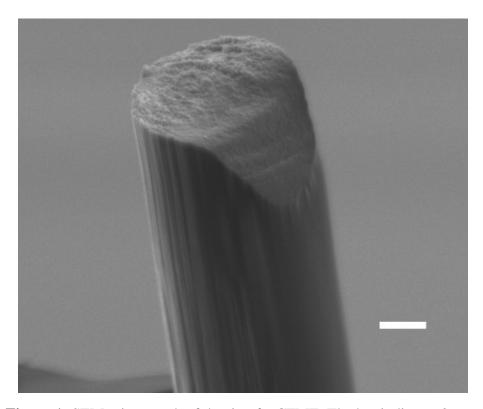


**Figure 1.** SEM micrograph of the tip of a CFME. The bar indicates 2  $\mu$ m.



Copyright©2025 by the authors. Published by ELSP. This work is licensed under a Creative Commons Attribution 4.0 International License, which permits unrestricted use, distribution, and reproduction in any medium provided the original work is properly cited.

#### 2. Impact of vertices on the capacitive current

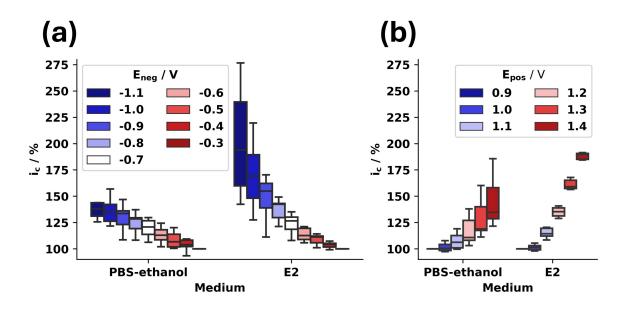


**Figure 2.**  $i_c$  increasing for more positive  $E_{pos}$  and more negative  $E_{neg}$ , compared in different medium 1% ethanol in PBS, and 0  $\mu$ M of E2, with CV.

#### 3. Influence of cathodic vs. anodic electrode pre-treatment on $i_c$ and $E_{ox,E2}$

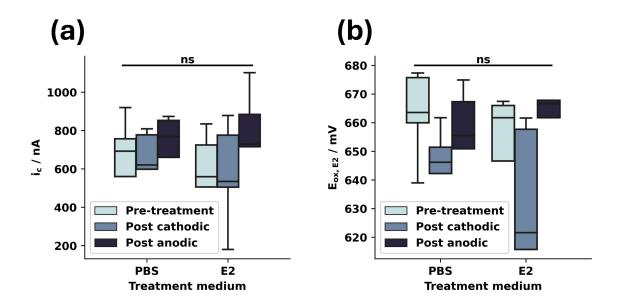


**Figure 3.** No significant variation for  $i_c$  or  $E_{ox,E2}$  when applying cathodic and anodic pre-treatments, both in 10  $\mu$ M E2 and in PBS.

#### 4. Influence of the holding potential on the E2 peak current in FSCV

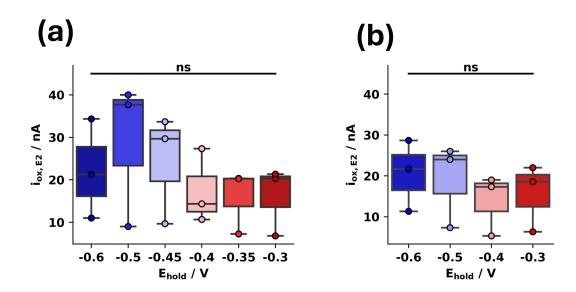


**Figure 4.** No significant variation for  $i_{ox,E2}$  when decreasing the holding potential  $E_{hold}$  in FSCV E2 detection, for a swithcing potential  $E_{switch}$  of (a) 1.45 V and (b) 1.35 V.

#### 5. Calibration curve for E2

To better characterize the FCSV system, a calibration curve was built for the waveform defined above  $(E_{shift} = 1.45 \text{ V}, E_{hold} = -0.35 \text{ V})$  as shown in Figure 5(a). A linear increase in current is observed as [E2] increases up to 10  $\mu$ M (Figure 5(b)). Above this concentration, the increase is sub-linear. This is due to the limited solubility of E2 in aqueous conditions, as E2 aqueous solubility is ~10  $\mu$ M [1]. It is expected that the slower increase in current above the solubility limit is due to the local solubilization of E2 as freely diffusing E2 molecules are irreversibly oxidised by the CFME. To better describe this behavior, a model smilar to a Langmuir isotherm model was used to fit  $i_{ox}$  as a function of [E2]. This model is typically used to describe the adsorption of freely diffusing molecules on a surface, and is therefore suitable for describing the saturation of the solution due to limited solubility.

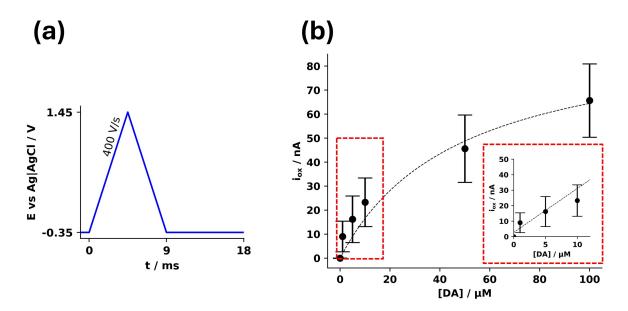


**Figure 5.** Calibration curve measurements using the FSCV. (a) The potential is varied from -0.35 V to 1.45 V and back, at a SR of 400 V.s<sup>-1</sup> with a frequency of 10 Hz. (b) The obtained calibration curve for several E2 concentrations. The main figure shows the langmuir behavior and the inset highlights the linear range. n = 5.

The sub-10  $\mu$ M range was fit with a linear model (Figure 5(b), inset). The sensitivity (*i.e.* the slope of the curve) was  $2.66 \pm 1.09 \text{ nA}.\mu\text{M}^{-1}$  (for n = 5). The LoD, defined as the concentration associated by the calibration curves to 3 times the standard deviation of the blank added to the blank signal, was  $500.07 \pm 234.55 \text{ nM}$  (n = 5). Other studies reported a LoD in the 10 nM range [2]. The higher value found here is likely due to differences in experimental set-up, in particular the hydrodynamic conditions encountered in the microfluidic test chambers. Finite element modelling (FEM, see the Supplementary Information) simulations of the fluidic conditions in the chamber reveals a strong gradient in fluid velocity close to the inlet, where the electrode was placed. As the local fluid velocity U controls the Faradaic current through constriction of the viscous boundary layer, the recorded signal is strongly dependent on electrode placement, *etc*. Consequently, the LoD, which is basically the noise divided by the sensitivity (signal) is largely influenced by the changes in the velocity field, which largely accounts for the differences observed here.

#### 6. Calibration curve for DA FSCV

Figure 6 displays a calibration curve computed for DA in PBS, using FSCV, for 3 electrodes. The LoD was  $52.87 \pm 22.99$  nM, and the sensitivity was  $25.41 \pm 1.42$  nA. $\mu$ M<sup>-1</sup>.

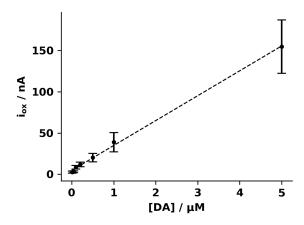


**Figure 6.** Calibration curve for the FSCV detection of DA, in PBS, for 3 electrodes. The data is presented as mean  $\pm$  SD.

#### 7. FSCV of other neurotransmitters and molecules of the brain

To highlight the possibility of detecting, identifying and resolving several neurotransmitters or molecules in the brain with an unmodified electrode, the FSCV protocol was repeated for several molecules of neurochemical significance. 5-HT and OA are neurotransmitters (Figure 7 and Figure 8), and AA is a redox molecule present in high concentration in the brain (Figure 9). For all these molecules, CV traces could be acquired, and the shapes of these CV allow the identification of a specific molecule.

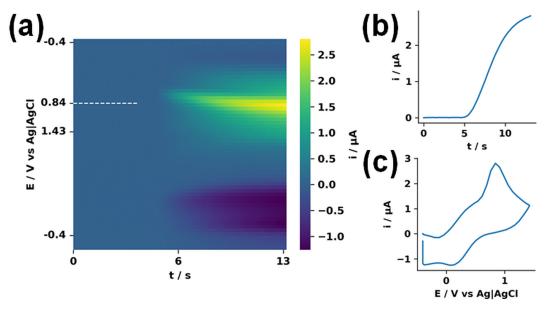


**Figure 7.** FSCV detection of 5-HT. (a) Typical FSCV data for  $10\mu$ M 5-HT in PBS with (b) the time evolution of the peak current at the potential indicated by the white dotted line and (c) the CV extracted from the point of maximum peak current.

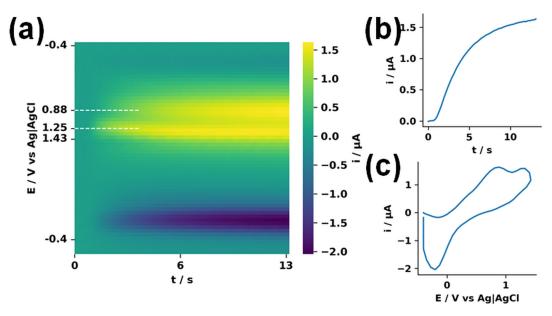


**Figure 8.** FSCV detection of OA. (a) OA5-HT in PBS with (b) the time evolution of the peak current at the potential indicated by the white dotted line and (c) the CV extracted from the point of maximum peak current.

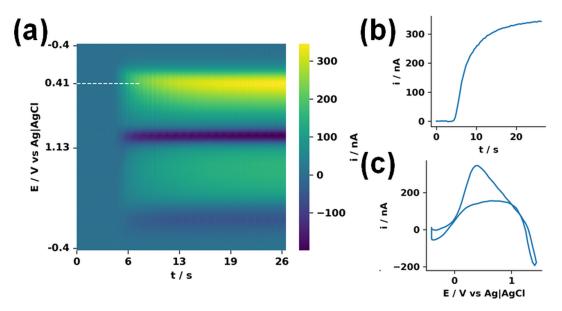


**Figure 9.** FSCV detection of AA. (a) Typical FSCV data for 1 mM AA in PBS with (b) the time evolution of the peak current at the potential indicated by the white dotted line and (c) the CV extracted from the point of maximum peak current.

#### 8. Simulation of the microfluidic chip

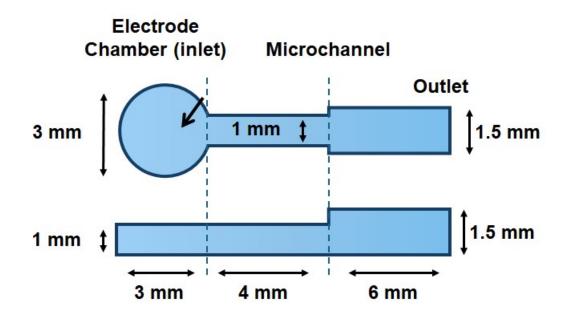


**Figure 10.** Schematics of the channel dimension in the microfluidic chip. The black arrow indicates the approximate position of the CFME during the tests.

As explained in the main text, a microfluidic chip was built to run the FSCV tests. In all the tests, the flow rate was maintained at 1 ml.min<sup>-1</sup>. The channel itself was made from PDMS using standard soft lithographic techniques. The mold was made using a desktop 3D printer, featuring the channel presented in Figure 10. The CFME was placed in the lumen of this channel to run the test, with the sensing part being located in the 3-mm disk, as indicated by the black arrow. The inlet port was cut with a 1-mm biopsy punch, at the center of the electrode chamber. A section of tubing was fitted to this port to connect the chip to a syringe pump.

Finite element modeling (FEM) simulations were run with COMSOL. The fluidic system was designed as displayed in Figure 11. A flow rate of 1 ml.min<sup>-1</sup> was applied to the inlet. The system was solved for a laminar flow of water, and the stationary state was considered.

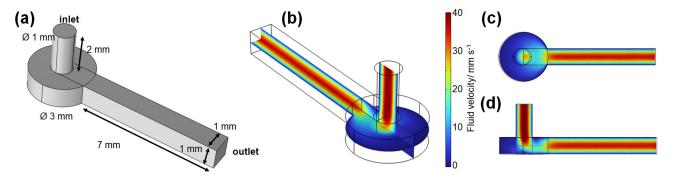


**Figure 11.** FEM modeling of the fluidic chamber. (a) Geometry of the model. (b) Results of the simulation of the fluid velocity, with projections over (c) the xy and (d) yz planes.

As shown in Figure 11(b)–(d), large variations in fluid velocity can be observed in the circular chamber close to the inlet, where the electrode was placed. This can impact the electrochemical response of the sensor, as discussed in the main manuscript.

#### 9. E2 detection methods

Table 1 summarizes some of the most common method available for detecting E2. It also highlights different parameters, especially the possibility to run real-time measurements, to better underline the advantages of FSCV.

**Table 1.** Comparative summary of some of the most common techniques for E2 detection.

Detection method		LoD (DA)	LoD (E2)	In vivo real-time analysis	Affordability
Immunoassays	RIA ELISA	17.4 pM [3]	No 1.5 nM [4]	No No	Expensive, complex
minunoussuys	CLIA	17.4 pm [3]	No	No	equipment
Mass spectrometry		1.3 nM [5]	367 pM [6]	No	Expensive, complex equipment
LC, GC or HPLC		26 pM [7]	37-92 nM [8]	No, except if coupled with microdialysis (temporal resolution > min)	Expensive, complex equipment
Biosensors		19 nM	37 nM	Possible	Fabrication can be difficult and/or expensive
Electrochemistry	DPV, CV, SWV FSCV	0.62 nM [9] 15 nM [11]	0.2 μM to 0.5 fM [10] 31.2 nM [12]	No Temporal resolution < 100 ms	Cheap, easy-to-use, sustainable

RIA: Radio immunoassay; ELISA: Enzyme-linked immunosorbent assay; CLIA: Chemiluminescence immunoassay; LC: liquid chromatography; GC: gas chromatography; HPLC: high-performance liquid chromatography.

#### References

- [1] Yalkowsky SH, He Y, Jain P. *Handbook of Aqueous Solubility Data*, 2nd ed. Boca Raton: CRC Press, 2003.
- [2] Weese-Myers ME, Ross AE. Electrochemical characterization of  $17\beta$ -estradiol with fast-scan cyclic voltammetry. *Electroanalysis* 2023, 35(9):e202200560.
- [3] Dopamine ELISA kit Ultra-Sensitive Any sample, Available = https://www.immusmol.com/shop/dopamine-elisa-kit-any-sample/ (accessed on 17 July 2024).
- [4] Huang Y, Zhang L, Li ZZ, Gopinath SCB, Chen Y, *et al.* Aptamer–17β-estradiol–antibody sandwich ELISA for determination of gynecological endocrine function. *Biotechnol. Appl. Biochem.* 2021, 68(4):881–888.
- [5] Davla S, Daly E, Nedow J, Gritsas A, Curran L, *et al.* An LC-MS/MS method for simultaneous analysis of up to six monoamines from brain tissues. *J. Chromatogr. B* 2023, 1216:123604.
- [6] Yilmaz B, Kadioglu Y. Determination of 17  $\beta$ -estradiol in rabbit plasma by gas chromatography with flame ionization detection. *Indian J. Pharm. Sci.* 2012, 74(3):248.
- [7] Qi D, Zhang Q, Zhou W, Zhao J, Zhang B, *et al.* Quantification of dopamine in brain microdialysates with high-performance liquid chromatography–tandem mass spectrometry. *Anal. Sci.* 2016, 32(4):419–424.
- [8] Yilmaz B, Kadioglu Y. Determination of 17  $\beta$ -estradiol in pharmaceutical preparation by UV

- spectrophotometry and high performance liquid chromatography methods. *Arab. J. Chem.* 2017, 10:S1422–S1428.
- [9] Luo H, Zhao YY, Jin XY, Yang JM, Cong H, *et al.* Voltammetric detection of catechol and dopamine based on a supramolecular composite prepared from multifarene [3, 3] and reduced graphene oxide. *Electroanalysis* 2020, 32(7):1449–1458.
- [10] Chang Z, Zhu B, Liu J, Zhu X, Xu M, *et al.* Electrochemical aptasensor for  $17\beta$ -estradiol using disposable laser scribed graphene electrodes. *Biosens. Bioelectron.* 2021, 185:113247.
- [11] Puthongkham P, Yang C, Venton BJ. Carbon nanohorn-modified carbon fiber microelectrodes for dopamine detection. *Electroanalysis* 2018, 30(6):1073–1081.
- [12] Weese-Myers ME, Ross AE. Subsecond codetection of dopamine and estradiol at a modified sharkfin waveform. *Anal. Chem.* 2024, 96(1):76–84.